Assembly, Two-Photon Absorption, and Bioimaging of Living Cells of A Cuprous Cluster

ARTICLE *in* CHEMISTRY OF MATERIALS · DECEMBER 2011

Impact Factor: 8.35 · DOI: 10.1021/cm2029855

13 AUTHORS, INCLUDING:

Xiaohe Tian
Anhui University
19 PUBLICATIONS **159** CITATIONS
SEE PROFILE

Qiong Zhang
MinNan Normal University
55 PUBLICATIONS **393** CITATIONS
SEE PROFILE

Hongping Zhou
Anhui University
96 PUBLICATIONS **693** CITATIONS
SEE PROFILE

Baokang Jin
Anhui University
70 PUBLICATIONS **842** CITATIONS
SEE PROFILE

CHEMISTRY OF MATERIALS

Article

pubs.acs.org/cm

Assembly, Two-Photon Absorption, and Bioimaging of Living Cells of A Cuprous Cluster

Xuchun Wang,[†] Xiaohe Tian,[‡] Qiong Zhang,[†] Pingping Sun,[†] Jieying Wu,[†] Hongping Zhou,[†] Baokang Jin,[†] Jiaxiang Yang,[†] Shengyi Zhang,[†] Chuankui Wang,[∥] Xutang Tao,[§] Minhua Jiang,[§] and Yupeng Tian*[,†,§,⊥]

[†]Department of Chemistry, Key Laboratory of Functional Inorganic Materials Chemistry of Anhui Province, Anhui University, Hefei, 230039, P. R. China

[‡]Department of Biomedical Science, University of Sheffield, Sheffield, United Kingdom

[§]State Key Laboratory of Crystal Materials, Shandong University, Jinan, 250100, P. R. China

[∥]Department of Physics, Shandong Normal University; Jinan 250014, P. R. China

[⊥]State Key Laboratory of Coordination Chemistry, Nanjing University, Nanjing, 230039, P. R. China

Supporting Information

ABSTRACT: A novel cuprous(I) cluster $Cu_4I_4L_4$ (L = (*E*)-(4-diethylanilino-styryl)pyridine) bearing strong two-photon absorption (TPA) was obtained using a facile assembly method, and the crystal structure has been determined. Quantum chemical calculations using time-dependent density functional theory (TD-DFT) reveals that the combination of the organic ligands with the three-dimensional Cu_4I_4 core extends the electronic delocalization in the cluster, leading to strong two-photon absorption action. The TPA cross sections ($\Phi\sigma_2$) of $Cu_4I_4L_4$ were enhanced with increasing polarity of solvents, which is quite different from the solvent effects on TPA in the literature. Compared to its free ligand, the cluster $Cu_4I_4L_4$ exhibits larger peak TPA cross sections in the near-infrared region, longer fluorescence lifetimes, higher quantum yield and photostability, lower cytotoxicity, and brighter two-photon fluorescent (TPF) bioimaging. These integrated advantages make it desirable to be applied as a two-photon fluorescent probe for labeling the nucleic acids in live cells.

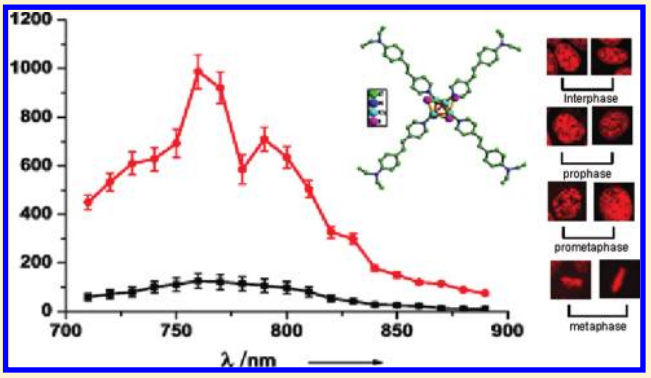

KEYWORDS: *assembly, two-photon absorption, bioimaging, cuprous cluster*

Molecules with large two-photon absorption (TPA) cross sections (σ_2) have attracted considerable interests because of their significant applications in the areas of nonlinear optical (NLO) materials,[1,2] such as two-photon excited fluorescence (TPEF) microscopy,[3,4] optical limiting,[5] optical data storage,[6] optical computing,[7] photodynamic cancer therapy,[8] and two-photon fluorescent (TPF) probes.[9−11] One of the most significant advantages of TPA materials in practical applications is the two-photon microscopy (TPM), which offers a number of advantages in biological imaging, including reduced phototoxicity, increased penetration depth, and negligible background fluorescence.[3,12−14] However, a highly efficient TPF probe that can reflect the cell environment accurately is rare, because there are three essential requirements for an ideal TPF probe. First, the receptor should have strong affinity with special species. Second, the fluorescence signal should not be perturbed by the environment.[9−11,15−17] Third, large σ_2 was required. Fourthly, the probe should not interfere with the cell and its properties. In current research in the field of TPA materials, well-accepted design approaches to achieve large σ_2 are generally based on the introduction of an electron donor and acceptor to the ends of a π-conjugated system.[1,2] The results of these studies, as well as theoretical calculation, reveal that σ_2 values increase on proceeding from dipolar to multipolar molecules and also with increasing donor and acceptor strength.[2,18] However, the synthesis of multipolar molecules having π-conjugated motifs incorporating donor and acceptor moieties requires significant synthetic skills and generally affords very low yields of the desired products.

The coordination clusters are reported to be excellent candidates for NLO materials because they involve $d\pi-p\pi$ delocalized systems and $d\pi-d\pi$ conjugated systems.[19,20] These clusters have a large variety of structures and diverse electronic properties that can be tuned by virtue of the coordinated metal

Special Issue: Materials for Biological Applications

Received: October 3, 2011
Revised: December 13, 2011
Published: December 13, 2011

ions.[20,21] The clusters can also extend the electronic delocalization, which should increase their σ_2 values. Hou et al. found that both metal ions and organic ligands are important for the NLO properties of such clusters.[22] However, the NLO properties of most clusters have been investigated with laser pulses of wavelength at 532 nm,[20] no organic−inorganic hybrid cluster with TPA in the near-IR region (700−900 nm) as well as specific labeling ability has been reported up to now, according to our knowledge.

We have paid attention to enhance σ_2 value by combining the functional ligands with metal clusters. Copper(I) iodide (CuI) clusters can be used as precursors to react with the bulky ancillary organic ligands, which are favorable for the formation of multibranched clusters with large σ_2 in the near-IR region. This is most likely due to the following three facts: (i) the closed-shell d^{10} Cu(I) shows a variety of coordination formats; (ii) CuI shows higher energy emission bands than its polymorphs (CuBr, CuCl)[23] and can be facilely modified varying with structure; and (iii) the multibranched cluster can extend electronic delocalization and polarity of rigid conjugated structural motifs (organic ligand) that would favor intra/intermolecular charge transfer and thus help to enhance TPA. With the above considerations, the authors designed a novel multibranched cuprous cluster ($Cu_4I_4L_4$, L = (*E*)-(4-diethylanilino-styryl)pyridine, Scheme 1) possessing larger conjugation motifs to enhance TPA for a brighter TPM image.

Scheme 1. Molecular Structure of $Cu_4I_4L_4$

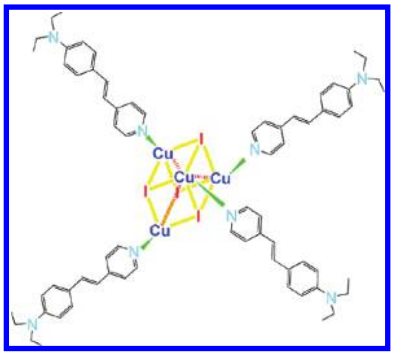

RESULTS AND DISCUSSION

Structure Investigation and Computational Details for $Cu_4I_4L_4$. The cluster $Cu_4I_4L_4$ was obtained as red-brown needle crystals through slowly evaporating a mixture of the newly synthesized copper(I) iodide and the ligand in acetonitrile. Its structure was confirmed by IR, ^{1}H NMR, and ^{13}C NMR spectra and elemental analyses. The coordinated pyridine groups led to their IR spectral bands shifting to higher frequency compared with those of the free ligands. The ^{1}H NMR spectrum of $Cu_4I_4L_4$ displays well resolved peaks, ranging from 5.7 to 8.4 ppm. Compared with those in free ligands, their positions in $Cu_4I_4L_4$ were shifted to lower fields. The ^{1}H NMR spectra at varied temperatures indicate that the well resolved peaks of the spectra exhibit almost no change in the temperature range −10−30 °C (Figure 5), which proved that the solid structure of $Cu_4I_4L_4$ is still kept in solution.

As shown in Figure 1a, it can be seen that the core of $Cu_4I_4L_4$ consists of four Cu and four I atoms. Average distances of Cu−I, Cu−N, Cu···Cu, and I···I in the core are 2.70, 2.04, 2.72, and 4.48 Å, respectively, which are in agreement with those of the

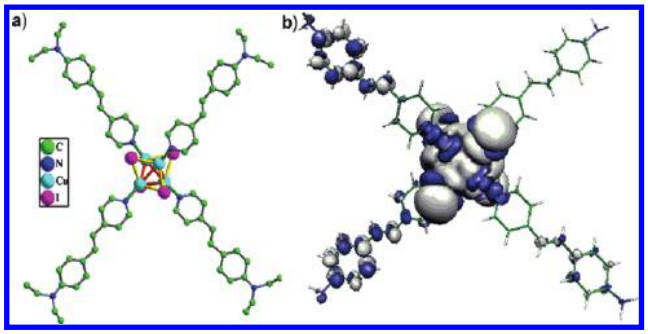

Figure 1. (a) Crystal structure of $Cu_4I_4L_4$. (b) Charge-transfer density difference of $Cu_4I_4L_4$ in the gas phase, areas with criss-cross marking and dots represent electron loss and gain, respectively.

reported [CuI(4-tert-butylpyridine)]$_4$ tetramer.[24] Notably, the Cu−Cu distances all fall in the range 2.64−2.73 Å (Table S2, Supporting Information) and are shorter than the sum of the van der Waals radii (2.80 Å). The shorten Cu−Cu distances can be attributed to the large anionic iodides, which force the copper atoms together, and the bonding is mainly electrostatic, with partial metal−metal bonds.[23−25] The average distance (1.290 (5) Å) of the bridge C═C bond of the coordinating Ls in $Cu_4I_4L_4$ is shorter than its value (1.325(6) Å) in the free L. Interestingly, the ligands oriented at diagonal positions in the four-branch cluster are almost coplanar with the torsion angle from 156° to 172°.

To better understand the charge transfer state, density functional theory (DFT) calculations on $Cu_4I_4L_4$ were carried out.[26] The molecular geometry optimization used for the calculation is obtained from single crystal X-ray diffraction crystallographic data. From Figure 1b, it can be seen that charges upon the excitation are mainly transferred from the two branches to the center, thus there are more electrons on average at the cluster center in the charge transfer (CT) state. Further studies have shown that the 324 highest occupied molecular orbitals (HOMOs) at S_0 state optimized geometry are combinations of copper d and iodine p orbitals, with pyridine-based bonding orbitals lying at lower energies (Tables 1 and 2; Figure S3, Supporting Information). Among the occupied states based on copper and iodine orbitals, those belonging to the HOMO/HOMO-3 and HOMO-5 set are mainly composed of iodine lone pairs with smaller contributions coming from antibonding copper d_z^2 and nitrogen lone pairs combinations. The 325 lowest unoccupied molecular orbitals (LUMOs) are two groups of almost degenerate π^* orbitals of the pyridine ligands. Notably, this orbital has bonding character among the four Cu atoms and antibonding character between all the Cu and I atoms.[27] Along with the results of the theoretical calculation, the functional chromophore L possesses a much larger conjugated framework and stronger push−pull effect compared with 4-tert-butylpyridine in [CuI(4-tert-butylpyridine)]$_4$.[24] The combination of L and Cu_4I_4 greatly extends electronic delocalization within the cluster (Figure 1b; Figure S3, Supporting Information), thus benefiting excited-state charge redistribution and NLO response to $Cu_4I_4L_4$.[28,29]

Linear Absorption and Single-Photon Excited Fluorescence (SPEF) of $Cu_4I_4L_4$. Figure 2 shows the single photon absorption (SPA) spectra and single-photon excited fluorescence (SPEF) spectra of $Cu_4I_4L_4$ and free L. As shown in Figure 1b, the electrons delocalize over the center, which reveals that $Cu_4I_4L_4$ could yield the desired photophysical

dx.doi.org/10.1021/cm2029855 | *Chem. Mater.* 2012, 24, 954−961

Table 1. Ab Initio Calculation Data of Single-Photon Excited Fluorescence, Energy Gap of the HOMO and LUMO, Oscillator Strengths of L and $Cu_4I_4L_4$ in Various Solvents

solvent	$\lambda_{ex\text{-}SPF}$ (nm)	E(LUMO-HOMO) (eV)	oscillator strengths	nature of the transition
ethanol	426.3[a]	2.9081	1.4212	68 (H) → 69 (L) (0.618)
	445.3	2.7829	0.0060	324 (H) → 325 (L) (0.701)
THF	426.2	1.4298	2.9092	68 (H)→69 (L) (0.619)
	446.2	2.7787	0.0027	319 (H-5) →325 (L) (0.540)
				324 (H)→325 (L) (−0.359)
$CHCl_3$	426.5	1.4372	2.9071	68 (H)→69 (L) (0.620)
	456.8	2.7142	0.0032	319 (H-5) →325 (L) (0.618)
				321 (H-3)→325 (L) (0.283)
benzene	424.4	1.4474	2.9219	68 (H)→69 (L) (0.676)
	445.4	2.7814	0.0024	321 (H-3)→325 (L) (0.459)
				324 (H)→325 (L) (0.311)
DMSO	432.3	2.8682	1.4533	68 (H)→69 (L) (0.621)
	446.3	2.7778	0.0010	324 (H)→325 (L) (0.702)

[a]For every solvent, the upper row is the data of L and the lower row is the data of $Cu_4I_4L_4$.

Table 2. Ab Initio Calculation Data of Single-Photon Excited Fluorescence, Two-Photon Excited Fluorescence Spectra, Energy Gap of the HOMO And LUMO, Oscillator Strengths, and TPA Cross Section in Gas State of L and $Cu_4I_4L_4$

	$\lambda_{ex\text{-}SPF}$ (nm)	$\lambda_{ex\text{-}TPF}$ (nm)	E(LUMO-HOMO) (eV)	oscillator strengths	σ_2 GM	nature of the transition
L	363.2	764.8	3.242	0.27	535	68(H)→69(L) (0.675)
$Cu_4I_4L_4$	390.9	780.5	3.17	0.057	2850	324(H-4)→326 (L) (0.639)

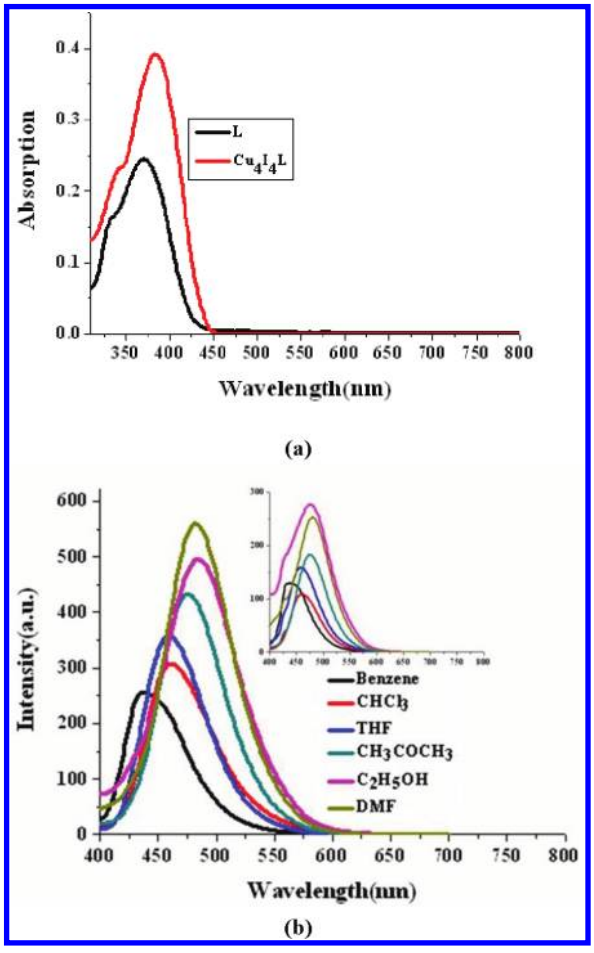

Figure 2. (a) Single-photon absorption spectra (SPA) (c = 1.0 × 10^{-5} mol L^{-1}, the spectra of inset) in ethanol solvent. (b) Single-photon excited fluorescence (SPEF) spectra of $Cu_4I_4(L)_4$ and L (the inset spectra) in six solvents (ex: 380 nm, c = 1.0 × 10^{-5} mol L^{-1}).

properties (absorption and fluorescence) dependent on the L ligand.

The SPA band between 300 and 450 nm of $Cu_4I_4L_4$ results mainly from the absorptive transition from the ground state S_0 to the S_1 state, which undergoes efficient vibrational relaxation upon one-photon excitation.[30] $Cu_4I_4L_4$ shows a weak positive solvatochromic (4−16 nm) absorption behavior, as a result of no significant permanent ground-state dipole moment in polar solvents (Figure 2a), while the fluorescence process has different characteristics. A marked red shift of the emission band with increasing polarity was shown in Figure 2b. Such behavor is consistent with a symmetry breaking in the relaxed excited state and the enhanced dipole−dipole interactions, leading to a more significant energy level decrease for polar emitting excited states.[31] The emission energy band, measured around 450 nm (calculated 324 HOMO → 325 LUMO, etc.), is due to a ^{3}XLCT excited state, which is in good agreement with related reported.[25] Note, the fluorescence quantum yields of $Cu_4I_4L_4$ not only increase nearly one-third compared with that of L (Table 3) but also exhibit obvious increase with increasing solvent polarity from benzene to ethanol, which could be explained by the hydrogen bonds of polar solvents consuming some energy from the excited state molecules.[25] The fluorescence lifetimes of $Cu_4I_4L_4$ in the four different solvents were increased by two to four times, compared with those of L (Table 3; Figure S4, Supporting Information), because the higher delocalization in $Cu_4I_4L_4$ results in more stabilization of the excited state of the aromatic arylamino groups. These results prove that the enhanced dipole−dipole interactions caused by the increasing polarity of the solvent lead to significant variations of red-shift, higher quantum yields, and longer fluorescence lifetimes.[32]

Two-Photon Absorption Characters of $Cu_4I_4L_4$. The TPA spectra of the $Cu_4I_4L_4$ and L were recorded in five solvents of differing polarity by two-photon excited fluorescence (TPEF) measurements in the range 700−900 nm. The spectra obtained by using the optimal excitation wavelength

dx.doi.org/10.1021/cm2029855 | Chem. Mater. 2012, 24, 954−961

Table 3. Data of Absorption Spectra, Single-Photon Excited Fluorescence, and Two-Photon Excited Fluorescence Spectra with Solvent Effects

solvent	n^a	ε^a	Δf	λ_{abs} (nm)	$\lambda_{em\text{-}SPF}$ (nm)	$\Delta\nu \times 10^3$ (cm^{-1})	Φ	τ (ns)	$\lambda_{em\text{-}TPF}$ nm	$\Phi\sigma_2{}^b$
ethanol	1.36	25.7	0.290	371[c]	475	5.08	0.39	0.16	488	124 ± 12
				387	486	6.45	0.72	3.25	491	995 ± 99
DMF	1.43	36.7	0.275	373	479	5.09	0.32	3.49	497	104 ± 10
				385	483	6.10	0.59	6.64	503	421 ± 42
THF	1.42	5.44	0.121	372	455	4.26	0.24	0.78	493	42 ± 4
				381	460	5.14	0.45	2.35	578	114 ± 11
$CHCl_3$	1.47	4.81	0.203	371	458	4.55	0.31	0.53	490	44 ± 4
				379	462	5.16	0.56	2.27	581	129 ± 13
benzene	1.50	2.28	0.003	373	432	3.10	0.15	0.05	453	16 ± 2
				381	442	4.32	0.25	2.14	475	53 ± 5

[a]The values of the refractive index (n) and dielectric constant (ε) are taken from *CRC Handbook of Chemistry and Physics,* 73rd ed.; CRC Press: Boca Raton, FL, 1992−1993. [b]GM = 1.0×10^{-50} cm^4 s $photon^{-1}$ $molecule^{-1}$. [c]For every solvent, the upper row is the data of L and the lower row is the data of $Cu_4I_4L_4$.

760 nm are shown in Figure 3a. In all the cases, the output intensity of two-photon excited fluorescence was linearly dependent on the input laser, thereby confirming the TPA process (Figure S4, Supporting Information). The TPEF spectra of the samples were compared with a reference solution of fluorescein at the corresponding excitation wavelengths. The TPA cross sections (σ_2) of $Cu_4I_4L_4$ and L were obtained by a comparison of the TPEF spectra of target molecules with fluorescein in a calibration standard.[33] The details of determination conditions and theoretical calculations are given in the Experimental Section.

From Figure 3a it is clear to see that the two-photon excited fluorescence (TPEF) peak positions of $Cu_4I_4L_4$ show a red-shift, compared to SPEF fluorescence, depending on the solvent polarity. All the spectra exhibited a broad emission band, and the emission maximum shifted to longer wavelengths with the increase of the solvent's polarity. For their TPEF spectra, large differences are observed between the cluster and its free ligand, which may arise from their different electronic structure, as a result of the ligands bonded to the cluster core to form a novel extended π-conjugated system in the $Cu_4I_4L_4$ molecule. The drastic solvatochromism can be explained by the effect of symmetry breaking, which leads to stronger dipole−dipole interactions in high polar solvents than that in low polar solvents.[32] To our knowledge, this phenomenon has been scarcely reported up to now, and there have been few theoretical studies to address the solvent effect.

Figure 3b indicated that, in the measured range, the TPA cross-section ($\Phi\sigma_2$) and σ_2 values of $Cu_4I_4L_4$ were enhanced with increasing polarity compared to its free ligand, especially in ethanol. However, the most up-reported organic TPA materials exhibit peak TPA cross-section in toluene, CH_2Cl_2, $CHCl_3$, and THF[1a,2,33−35] (Table 3 and Figure 3c). Importantly, the peak TPA cross sections were in the near-infrared range. The enhanced trend observed in the experiments was consistent with above structural investigation and theoretical calculations (Table 2). This large TPA response comes from the marked core to periphery charge redistribution in $Cu_4I_4L_4$ upon photoexcitation.[31] Therefore, complexation with Cu(I) enhances the electron-acceptor character of the central pyridine group, which converts the ligand to a more strongly polarized D−π−A unit, making this cluster a potential candidate for TPA responses. It should be noted that this σ value exceeds that of many fluorophores widely used in biology, including fluorescein, BODIPY, DAPI, GFP, ZnSalens, or other complexes.[35−39] Significantly, compared those with its free L, not only do the $Cu_4I_4L_4$ bear larger $\Phi\sigma_2$ and σ_2 values but also the cluster exhibits higher quantum yield, longer lifetime in ethanol (Table 3), which spurred us further to explore its potential application in biological imaging.

Two-Photon Microscopy Biological Imaging Application of $Cu_4I_4L_4$. Cytotoxicity as a potential side effect of $Cu_4I_4L_4$ should be considered when interacting with living cells or tissues. The cell viability data for MCF-7 (human breast carcinoma) cells treated with $Cu_4I_4L_4$ and the ligand, as quantified by the MTT assay, represent an established method for cytotoxicity (Table S3, Supporting Information). These data indicated no high toxicity of the sub-band low-micromolar concentrations of $Cu_4I_4L_4$ and significantly lower cytotoxicity than its ligand. The low cytotoxicity of $Cu_4I_4L_4$ and its unusual two-photon luminescent properties make it a potential candidate as novel luminescence material for live cell imaging. Prior to the investigations on bioimaging in living cells for the cluster undertaken in this work, the interactions between $Cu_4I_4L_4$/L and calf-thymus DNA were verified by UV−vis, fluorescence, and circular dichroism spectra (Figures S5−S9, Supporting Information). Apparently, all the photophysical data exhibit that the $Cu_4I_4L_4$ can be bonded with DNA, leading to larger charge-transfer and more enhanced fluorescence.[40]

To demonstrate the potential applications of $Cu_4I_4L_4$ for TPM imaging in living cells, MCF-7 cells were cultured and stained with $Cu_4I_4L_4$. To minimize the side effects of organic solvent toward live cells, both the cluster and L were dissolved in DMSO at high concentration and diluted with phosphate buffer solution to a working concentration. TPEF images (Figure 4a and d) of each live cell were successfully taken and clearly display the nucleus structure. To determine the location of the luminescence, a traditional nuclear dye 4′,6-diamidino-2-phenylindole (DAPI) was also used. Parts a and b of Figure 4 show that the cluster molecules have been taken up by the cellular nuclei; Figure 4c reveals the TPA luminescence from chromosomes of cells that are undergoing interphase and mitotic phases. Control experiments for $Cu_4I_4L_4$ and DAPI images (Figure 4a; Figure S8, Supporting Information) indicate that there is no affection between the $Cu_4I_4L_4$ and DAPI. Hence, $Cu_4I_4L_4$ is clearly capable of detecting the nuclear section in MCF-7 cells. The excitation and emission wavelengths of $Cu_4I_4L_4$ probes are 780−800 and 685 nm, respectively, which can be attributed to excited-state equilibrium via intersystem crossing (ISC) and triplet energy transfer

dx.doi.org/10.1021/cm2029855 | *Chem. Mater.* 2012, 24, 954−961

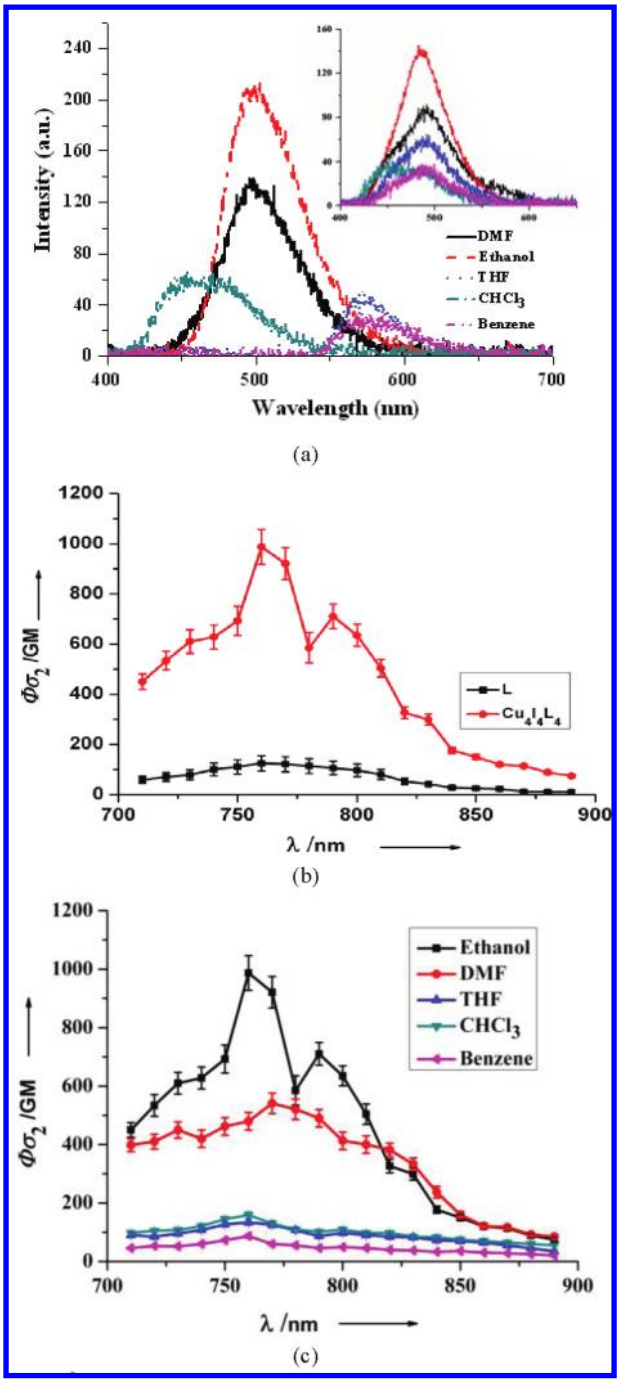

Figure 3. (a) Two-photon excited fluorescence (TPEF) spectra of $Cu_4I_4L_4$ and L (the spectra of inset) in five solvents (ex: 760 nm, c = 1.0 × 10^{-4} mol L^{-1}). (b) Two-photon absorption action spectra of L and $Cu_4I_4L_4$ in ethanol (c = 1.0 × 10^{-4} mol L^{-1}). (c) Two-photon absorption action spectra of $Cu_4I_4L_4$ in five solvents (c = 1.0 × 10^{-4} mol L^{-1}).

(TET),[41] and are different from that of the free ligand. Similar nuclear stain properties shown by L, using the same concentration (Figure 4d), however, show luminescence intensity to drop approximately 1/5 times lower than $Cu_4I_4L_4$ (Figure 4e). In addition, the cluster $Cu_4I_4L_4$ (200 μM) in MCF-7 nucleus region reveals higher stability upon laser irradiation during the period over 15 minutes (Figure S9, Supporting Information), which reveals almost no photobleaching. To further prove the stability of the cluster, the variable

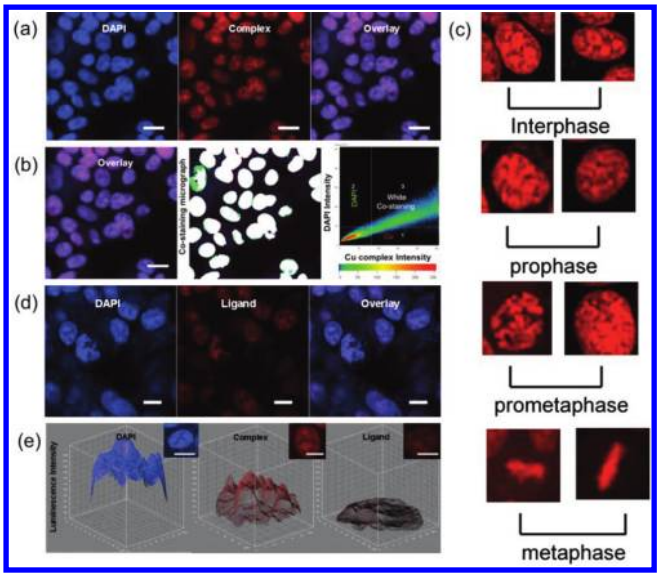

Figure 4. TPM of MCF-7: (a) containing $Cu_4I_4L_4$ (middle, red) with DAPI (left, blue) and overlay image (right); (b) colocalization micrograph profile proving that the costaining region 3 corresponds to the white colocalization part, which is located in nuclear section; (c) cell chromosome through progression of m-phase showing cellular luminescence by uptake cluster; (d) containing L (middle, red) with DPAI (left, blue) and overlay image. (e) 3D intensity profile of DAPI, $Cu_4I_4L_4$ (200 μM), and L (200 μM) luminescence across a MCF-7 single cell after incubation for 2 h. (All scale bars represent 10 μM.)

temperature ^{1}H NMR of $Cu_4I_4L_4$ has been measured (Figure 5). MALDI-TOF MS (matrix-assisted laser desorption

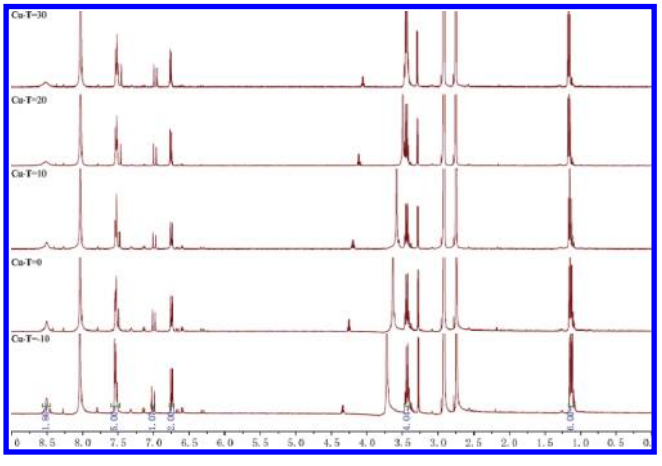

Figure 5. Variable temperature (−10−30 °C) ^{1}HNMR spectra of $Cu_4I_4L_4$.

ionization time-of-flight mass spectrometry) was used to further verify the stability of the cuprous cluster in water solution (Figure S10, Supporting Information), which was first dissolved in a small amount of DMF and then diluted with water. The results showed that $Cu_4I_4L_4$ is cell-permeable and suitable for nucleic acids staining and exhibits the high fluorescent sensitivity relative to L in live cells. The record TPA coefficient of $Cu_4I_4L_4$ and its application for *in vivo* two-photon imaging highlight the potential of the cuprous cluster.

In conclusion, a novel $Cu_4I_4L_4$ containing π-conjugated multibranches was designed and synthesized. The $Cu_4I_4L_4$ was investigated both experimentally and theoretically. The $Cu_4I_4L_4$

dx.doi.org/10.1021/cm2029855 | *Chem. Mater.* 2012, 24, 954−961

exhibits higher quantum yield, larger TPA cross section in the near-infrared region, higher photostability, and brighter two-photon fluorescent bioimaging than its free ligand, which make it successfully applied to a two-photon fluorescent probe for labeling the nucleic acids in live cells. Significantly, the cuprous cluster core can be tunable and the coordinating organic ligand can be tailored depending on special requirements, such as organo-/water-solublility and recognition. Further studies on this aspect are in progress in our laboratory. These explorations for the $Cu_4I_4L_4$ may provide a useful guide to the design of novel TPA materials.

EXPERIMENTAL SECTION

All chemicals were commercially available and used as obtained. The solvents were purified by conventional methods before use. Synthesis of (*E*)-(4-diethylanilinostyryl)pyridine (L) is available in the Supporting Information.

Synthesis of $Cu_4I_4L_4$. Fresh copper(I) iodide (0.38 g, 2 mmol) and the ligand (0.51 g, 2 mmol) were vigorously stirred in 15 mL of acetonitrile until the solid phase had been completely dissolved, and then, the mixture was refluxed for 2 h. The reaction mixture was cooled to room temperature and filtered into a large test tube. Red-brown needle crystals suitable for single crystal X-ray diffraction analysis were obtained by slow evaporation of acetonitrile solution of the complex at room temperature after a week. Yield: 88.70%. ^{1}H NMR (500 MHz, DMF-d_6, δ): 8.53 (s, 2H, py H), 7.55 (q, 5H, py and Ar H), 7.06 (d, 1H, CH═CH, H), 6.73 (d, 2H, Ar H) 3.43 (q, 4H, CH_2), 1.15 (q, 6H, CH_3). ^{13}C NMR (500 MHz, DMSO-d_6, δ): 148.55−148.46 (m, py), 140.57 (s, py), 129.34−127.22 (m, Ar), 111.93 (s, CH═CH), 44.22 (s, CH_2), 12.87 (s, CH_3). Anal. (%): C, 46.16; H, 4.51; N, 6.36. Found (%): C, 46.01: H, 4.55; N, 6.23.

General Instruments. Elemental analyses were performed on a Perkin−Elmer 240C elemental analyzer. IR spectra were recorded with a Nicolet FTIR Nexus 870 instrument in the range 4000−400 cm^{-1}, using KBr pellets. The mass spectra were obtained on a Micromass GCT-MS spectrometer and a Bruker reflex TOF mass spectrometer (Bruker-Franzen Analytik, Bremen, Germany). ^{1}H NMR spectra were performed on a Bruker AV 500 MHz Ultrashield spectrometer and were reported as parts per million (ppm) from TMS (δ). The single-photon absorption spectra were measured on a UV-265 spectrophotometer. The single-photon emission fluorescence (SPEF) spectra measurements were performed using Perkin−Elmer LS-55B fluorospectrometer. Fluorescence lifetime measurements were performed on a PicoQuant FluoTime 200 time-resolved fluorescence spectrometer by the time-correlated single-photon counting method (TCSPC) using a PDL 800-B picosecond diode Laser; a Hamamatsu R3809U-50 microchannel plate photomultiplier tube was used for detection. The decays were analyzed by "least-squares". The quality of the exponential fits was evaluated by the goodness of fit (χ^2).

Single-Crystal Structure Analysis. Single-crystal X-ray diffraction measurements were carried out on a Bruker Smart 1000 CCD diffractometer equipped with a graphite crystal monochromator situated in the incident beam for data collection at room temperature. The determination of unit cell parameters and data collections were performed with Mo Kα radiation (λ = 0.71073 Å). Unit cell dimensions were obtained with least-squares refinements, and all structures were solved by direct methods using SHELXL-97.[42] All non-hydrogen atoms were refined anisotropically. The hydrogen atoms were added theoretically and not refined. The final refinement was performed by full-matrix least-squares methods with anisotropic thermal parameters for non-hydrogen atoms on F^2. The crystallographic data for the cluster are listed in Table S2 in the Supporting Information. Selected bond lengths and angles are presented in Table S1 in the Supporting Information. CCDC-256603 for $Cu_4I_4L_4$ and CCDC-609933 for the ligand contain the supplementary crystallographic date for this paper. (These data can be obtained free of charge at www.ccdc.cam.ac.uk/conts/retrieving.html or from the Cambridge Crystallographic Data Centre, 12 Union Road, Cambridge CB2 1EZ, U.K. Fax: +44−1223/336−033. E-mail: deposit@ccdc.cam.ac.uk.)

Measurement of Two-Photon Excited Fluorescence and Two-Photon Absorption Cross Section. The two-photon emission fluorescence (TPEF) spectra were measured using a femtosecond Ti:sapphire laser (Coherent Mira 900F) as the pump source, with a pulse width of 200 fs and a repetition rate of 76 MHz, and a single-scan streak camera (Hamamatsu, model: C5680-01) together with a monochromator as the recorder. Circular dichroism spectra were measured using a JASCO J-820 CD spectrophotometer. The TPA cross sections (σ_2) of $Cu_4I_4L_4$ and L were obtained by the following equation and a comparison of the TPEF spectra of target molecules with fluoresce in the calibration standard.[32−34]

$$\sigma_2 = \frac{S_s}{S_r}\frac{\Phi_r N_r n_r}{\Phi_s N_s n_s}\sigma_r \quad (1)$$

Here, S is the integrated area under the corrected emission, Φ is the quantum yield (see the Supporting Information), N is the mol magnitude, n is the refractive index, subscripts s and r refer to the sample and reference solutions, respectively. The σ_r value of reference was taken from the literature.[33] The experimental errors of σ_2 values are estimated to be ±10%, as a result of variations of laser energies and sample concentrations.

The squared dependence of induced fluorescence power and incident laser intensity was observed, and the log−log plot of the fluorescence signal vs excited light power provided direct evidence for two-photon excited process (Figure S4, Supporting Information). However, with the increasing of incident irradiances, the power of emitting fluorescence deviated from the second-order power law and decreased gradually. This deviation may be attributed to some other nonlinear optical processes, such as stimulated emission, excited-state absorption, and ground-state depletion.[36,37]

Theoretical Calculation. Optimizations were carried out with B3LYP[LANL2DZ] without any symmetry restraint.[43] The time-dependent density functional theory (TD-DFT) {B3LYP-[LANL2DZ]} calculations were performed on the optimized structure.[44] All calculations, including optimizations and TD-DFT, were implemented with the G03 software.[26] Geometry optimization of the singlet ground state and the TDDFT calculation of the lowest 25 singlet−singlet excitation energies were carried out with a basis set composed of 6-31 G(d, p) for C, N, and H atoms[13a] and the Lanl2dz basis set for Cu and I atoms. The basis set was downloaded from the EMSL basis set library. An analytical frequency confirms evidence that the calculated species represents a true minimum without imaginary frequencies on the respective potential energy surface. The lowest 25 spin-allowed singlet−singlet transitions, up to energy of about 5 eV, were taken into account in the calculation of the absorption spectrum.

In terms of sum-overstate formula, the two-photon matrix element for the two-photon resonant absorption of identical energy is written as[43]

$$S_{\alpha\beta} = \sum_j \left[\frac{\langle 0|\mu_\alpha|j\rangle\langle j|\mu_\beta|f\rangle}{\omega_j - \omega_f/2} + \frac{\langle 0|\mu_\beta|j\rangle\langle j|\mu_\alpha|f\rangle}{\omega_j - \omega_f/2} \right] \quad (2)$$

where $|0\rangle$ and $|f\rangle$ denote the ground state and the final state, respectively. $|j\rangle$ represents the intermediate state and the ground state as well. ω_j is the excitation energy of the excited states, while μ is the electronic dipole moment. In general, the total TPA probability requires the information of all the excited states, which is not easy to obtain. On the other hand, a few-state model can often provide satisfactory results for TPA cross-section in a visible region.[45,46] The TPA cross-section is given by orientational averaging over the two-photon absorption probability.[47]

$$\delta_{tpa} = \sum_{\alpha\beta} [FS_{\alpha\alpha}S^*_{\beta\beta} + GS_{\alpha\beta}S^*_{\beta\beta} + HS_{\alpha\beta}S^*_{\beta\alpha}] \quad (3)$$

where the coefficients F, G, and H are related to the incident radiation. Values of F, G, and H are a constant of 2 in the linearly polarized light,

dx.doi.org/10.1021/cm2029855 | Chem. Mater. 2012, 24, 954−961

and −2, 3, and 3 in the circular case, respectively. In the present work, we only investigate the case with the linearly polarized laser beam. In eq 2 the summation goes over the molecular axes $\alpha, \beta = \{x, y, z\}$.

The TPA cross-section that is directly comparable with experimental measurements is defined as[48]

$$\sigma_{tp} = \frac{4\pi^2 a_0^5 \alpha}{15 c_0} \frac{\omega^2 g(\omega)}{\Gamma_f} \delta_{tp} \quad (4)$$

where a_0 is the Bohr radius; c_0 is the speed of light, α is the fine structure constant, and ω is the photon energy of the incident light. $g(\omega)$ denotes the spectral line profile, which is assumed to be a δ-function. Γ_f is the lifetime broadening of the final state, which is assumed to be 0.1 eV.

Cell Culture. Human breast carcinoma MCF-7 cells were maintained in RMPI 1640 medium supplemented with 2 mM L-glutamine, 100 IU mL^{-1} penicillin, 100 mg mL^{-1} streptomycin, and 10% fetal calf serum (FCS). Cultures were maintained at 37 °C in an atmosphere of 5% CO_2 and 95% air and subcultured routinely using 0.02% (w/v) EDTA once 80−95% confluence was achieved.

Cell Image. Cells were seeded in 6 well plates at a density of 2×10^5 cells per well and grown for 96 h. The cluster (and ligand) was dissolved in DMSO at high concentration in 20 mM and diluted by PBS (phosphate buffer solution) to working concentration. For live cell imaging, cell cultures were incubated with the cluster (10% PBS/90% cell media) at concentrations 200 μM and maintained at 37 °C in an atmosphere of 5% CO_2 and 95% air for incubation times ranging from 1 to 2 h. The cells were then washed with PBS (3 × 3 mL per well), and 3 mL of PBS was added to each well. The cells were imaged using confocal laser scanning microscopy and a water immersion lenses. Excitation energy of 780−800 nm was used, and the fluorescence emission measured at 650−700 nm. Costaining was performed using 200 nM DAPI for 10 min (in PBS).

Microscopy. MCF-7 cells were luminescently imaged on a Zeiss LSM 510 META upright confocal laser scanning microscope using magnification 40× and 100× water-dipping lenses for monolayer cultures. For DAPI excitation, a Coherent Chameleon pulsed infrared multiphoton laser was used (800 nm), and the emission was detected between 435 and 485 nm. Image data acquisition and processing was performed using Zeiss LSM Image Browser, Zeiss LSM Image Expert and Image J.

■ ASSOCIATED CONTENT

Supporting Information

Synthetic procedures and detailed experimental information; X-ray crystallographic data (CIF). This material is available free of charge via the Internet at http://pubs.acs.org.

■ AUTHOR INFORMATION

Corresponding Author

*Fax: 86-551-5107304. E-mail: yptian@ahu.edu.cn.

■ ACKNOWLEDGMENTS

This work was supported by the National Natural Science Foundation of China (21071001, 51142011), Ministry of Education Funded Projects focus on returned overseas scholar, The 211 Project of Anhui University, and Foundation of Scientific Innovation Team of Anhui Province (2006KJ007TD), Talent Foundation of Anhui Science and Technology University (ZRC2012313). The authors thank Dr. Guiseppe Battaglia, Dr. Jim A. Thomas, Dr. Xuanjun Zhang, Prof. Zhong-Lin Lu, and Dr. Longjiu Cheng for biological imaging and helpful discussions, respectively.

■ REFERENCES

(1) (a) He, G. S.; Tan, L. S.; Zheng, Q.; Prasad, P. N. *Chem. Rev.* **2008**, *108*, 1245−1330. (b) Hales, J. M.; Matichak, J.; Bredas, J. L; Perry, J. W.; Mader, S. R. *Science* **2010**, *327*, 1485−1488. (c) Haque, S. A.; Nelson, J. *Science* **2010**, *327*, 1466−1467.

(2) Pawlicki, M.; Collins, H. A.; Denning, R. G.; Anderson, H. L. *Angew. Chem., Int. Ed.* **2009**, *48*, 3244−3266.

(3) (a) Yuste, R. *Nat. Methods* **2005**, *2*, 902−913. (b) Helmchen, F.; Denk, W. *Nat. Methods* **2005**, *2*, 932−940.

(4) (a) Larson, D. R.; Zipfel, W.; Williams, R. M.; Clark, S. W.; Bruchez, M. P.; Wise, F. W.; Webb, W. W. *Science* **2003**, *300*, 1434−1436. (b) Gao, Y. H.; Wu, J. Y.; Li, Y.; Sun, P. P.; Zhou, H. P.; Yang, J. X.; Zhang, S. Y.; Jin, B. K.; Tian, Y. P. *J. Am. Chem. Soc.* **2009**, *131*, 5208−5213.

(5) Guda, R.; Oleg, V.; Lee, D.; Goodson, T. *J. Am. Chem. Soc.* **2008**, *130*, 5032−5033.

(6) Azijlstra, P.; James, W. M. C.; Gu, M. *Nature* **2009**, *459*, 410−413.

(7) Szacilowsk, K. *Chem. Rev.* **2008**, *108*, 3481−3548.

(8) (a) Ford, P. C. *Acc. Chem. Res.* **2008**, *41*, 190−200. (b) Starkey, J. R.; Rebane, A. K.; Spanger, C. W. *Clin. Cancer Res.* **2008**, *14*, 6564−6573. (c) Beverina, L.; Crippa, M.; Landenna, M.; Ruffo, R.; Pagani, G. A. *J. Am. Chem. Soc.* **2008**, *130*, 1894−1902.

(9) (a) Lee, J. H.; Lim, C. S.; Tian, Y. S.; Han, J. H.; Cho, B. R. *J. Am. Chem. Soc.* **2010**, *132*, 1216−1217. (b) Sumalekshmy, S.; Fahrni, C. J. *Chem. Mater.* **2011**, *23*, 483−500.

(10) Sumalekshmy, S.; Fahrni, C. *J. Chem. Mater.* **2011**, *23*, 483−500.

(11) (a) Masanta, G.; Lim, C. S.; Kim, H. J.; Han, J. H.; Kim, H. M.; Cho, B. R. *J. Am. Chem. Soc.* **2011**, *133*, 5698−5700. (b) Kim, H. M.; Cho, B. R. *Chem.—Asian J.* **2011**, *6*, 58−69.

(12) (a) Kim, M. K.; Lim, C. S.; Hong, J. T.; Han, J. H.; Jang, H. Y.; Kim, H. M.; Cho, B. R. *Angew. Chem., Int. Ed.* **2010**, *49*, 364−367. (b) Kim, H. J.; Han, J. H.; Kim, M. K.; Lim, C. S.; Kim, H. M.; Cho, B. R. *Angew. Chem., Int. Ed.* **2010**, *49*, 6786−6789. (c) Kim, H. M.; Seo, M. S.; An, M. J.; Han, J. H.; Tian, Y. S.; Choi, J. H.; Kwon, O.; Lee, K. J.; Cho, B. R. *Angew. Chem., Int. Ed.* **2008**, *120*, 5245−5248.

(13) (a) Li, D.; Tian, X.; Hu, G.; Zhang, Q.; Wang, P.; Sun, P.; Zhou, H.; Meng, X.; Yang, J.; Wu, J.; Jin, B.; Zhang, S.; Tao, X.; Tian, Y. *Inorg. Chem.* **2011**, *50*, 7997−8006. (b) Nuria, R.; Adrien, B.; Patrice, L. B.; Hubert, L. B.; Chantal, A.; Sophie, B.; Christophe, C.; Olivier, M. *Chem. Mater.* **2011**, *23*, 3228−3236. (c) Zhu, M. -Q.; Zhang, G.-F.; Li, C; Aldred, M. P.; Chang, E.; Drezek, R. A.; Li, A. D. Q. *J. Am. Chem. Soc.* **2011**, *133*, 365−372. (d) Law, G. L.; Wong, K. L.; Man, C. W. Y.; Wong, W. T.; Tsao, S. W.; Lam, M. H. W; Lam, P. K. S. *J. Am. Chem. Soc.* **2008**, *130*, 3714−3715.

(14) (a) Rendón, N.; Bourdolle, A.; Baldeck, P. L.; Bozec, H. L.; Andraud, C.; Brasselet, S.; Copéret, C.; Maury, O. *Chem. Mater.* **2011**, *23*, 3228−3236. (b) Biswas, S.; Wang, X.; Morales, A. R.; Ahn, H. -Y.; Belfield, K. D. *Biomacromolecules* **2011**, *12*, 441−449. (c) Zipfel, W. R.; Williams, R.; Webb, M. W. W. *Nat. Biotechnol.* **2003**, *21*, 1369−1377. (d) Montgomery, C. P.; Murray, B. S.; New, E. J.; Pal, R.; Parker, D. *Acc. Chem. Res.* **2009**, *42*, 925−937.

(15) (a) Kim, H. M.; Cho, B. R. *Acc. Chem. Res.* **2009**, *42*, 863−872. (b) Botchway, S. W.; Charnley, M.; Haycock, J. W.; Park, A. W.; Rochester, D. L.; Weinstein, J. A.; Gareth Williams, J. A. *Proc. Natl. Acad. Sci. U.S.A.* **2008**, *21*, 16071.

(16) (a) Xu, Z.; Baek, K. H.; Kim, H. N.; Cui, J.; Qian, X.; Spring, D. R.; Shin, I.; Yoon, J. *J. Am. Chem. Soc.* **2010**, *132*, 601−610. (b) Taki, M.; Wolford, J. L.; O'Halloran, T. V. *J. Am. Chem. Soc.* **2004**, *126*, 712−713.

(17) Jiang, P.; Guo, Z. *J. Coord. Chem. Rev.* **2004**, *248*, 205−229.

(18) Kim, H. M.; Cho, B. R. *Chem. Commun.* **2009**, 153−164.

(19) Zhang, C.; Cao, Y.; Zhang, J. F.; Humphrey, M. G. *Adv. Mater.* **2008**, *20*, 1870−1875.

(20) Zhang, C.; Song, Y. L.; Wang, X. *Coord. Chem. Rev.* **2007**, *251*, 111−141.

(21) Powell, C. E.; Morrall, J. P.; Ward, S. A.; Cifuentes, M. P.; Notaras, E. G.; Samoc, A. M.; Humphrey, M. G. *J. Am. Chem. Soc.* **2004**, *126*, 12234−12235.

(22) Hou, H. W.; Wei, Y. L.; Song, Y. L.; Mi, L. M.; Tang, M. S.; Li, L. K.; Fan, Y. T. *Angew. Chem., Int. Ed.* **2005**, *44*, 6067−6074.

(23) Ford, P. C.; Cariati, E.; Bourassa, J. *Chem. Rev.* **1999**, *99*, 3625−3648.
(24) Cariati, E.; Roberto, D.; Ugo, R.; Ford, P. C.; Galli, S.; Sironi, A. *Inorg. Chem.* **2005**, *44*, 4077−4085.
(25) Angelis, F. D.; Fantacci, S.; Sgamellotti, A.; Cariati, E.; Ugo, R.; Ford, P. C. *Inorg. Chem.* **2006**, *45*, 10576−10584.
(26) Frisch, M. J.; Trucks, G. W.; Schlegel, H. B.; Scuseria, G. E.; Robb, M. A.; Cheeseman, J. R.; Montgomery, J. A., Jr.; Vreven, T.; Kudin, K. N.; Burant, J. C.; Millam, J. M.; Iyengar, S. S.; Tomasi, J.; Barone, V.; Mennucci, B.; Cossi, M.; Scalmani, G.; Rega, N.; Petersson, G. A.; Nakatsuji, H.; Hada, M.; Ehara, M.; Toyota, K.; Fukuda, R.; Hasegawa, J.; Ishida, M.; Nakajima, T.; Honda, Y.; Kitao, O.; Nakai, H.; Klene, M.; Li, X.; Knox, J. E.; Hratchian, H. P.; Cross, J. B.; Adamo, C.; Jaramillo, J.; Gomperts, R.; Stratmann, R. E.; Yazyev, O.; Austin, A. J.; Cammi, R.; Pomelli, C.; Ochterski, J. W.; Ayala, P. Y.; Morokuma, K.; Voth, G. A.; Salvador, P.; Dannenberg, J. J.; Zakrzewski, V. G.; Dapprich, S.; Daniels, A. D.; Strain, M. C.; Farkas, O.; Malick, D. K.; Rabuck, A. D.; Raghavachari, K.; Foresman, J. B.; Ortiz, J. V.; Cui, Q.; Baboul, A. G.; Clifford, S.; Cioslowski, J.; Stefanov, B. B.; Liu, G.; Liashenko, A.; Piskorz, P.; Komaromi, I.; Martin, R. L.; Fox, D. J.; Keith., T.; Al-Laham, M. A.; Peng, C. Y.; Nanayakkara, A.; Challacombe, M.; Gill, P. M. W.; Johnson, B.; Chen, W.; Wong, M. W.; Gonzalez, C.; Pople, J. A. *Gaussian 03*, Revision B.04; Gaussian, Inc.: Pittsburgh, PA, 2003.
(27) Angelis, F. D.; Fantacci, S.; Sgamellotti, A.; Cariati, E.; Ugo, R.; Ford, P. C. *Inorg. Chem.* **2006**, *45*, 10576−10584.
(28) Malicki, M.; Hales, J. M.; Rumi, M.; Barlow, S.; McClary, L.; Marder, S. R.; Perry, J. W. *Phys. Chem. Chem. Phys.* **2010**, *12*, 6267−6277.
(29) Lin, H. C.; Kim., H.; Barlow, S.; Hales, J. M.; Perry, J. W.; Marder, S. R. *Chem. Commun.* **2011**, *47*, 782−784.
(30) Zheng, Q. D.; He, G. S.; Prasad, P. N. *J. Mater. Chem.* **2005**, *15*, 579−587.
(31) Katan, C.; Charlot, M.; Mongin, O.; Droumaguet, C.; Jouikov, V.; Terenziani, F.; Badaeva, E.; Tretiak, S.; Blanchard-Desce, M. *J. Phys. Chem. B* **2010**, *114*, 3152−3169.
(32) Noh, S. B.; Kim, R. H.; Kim, W. J.; Kim, S.; Lee, K.-S.; Cho, N. S.; Shim, H. K.; Pudavar, H. E.; Prasad, P. N. *J. Mater. Chem.* **2010**, *20*, 7422−7429. (b) Terenziani, F.; Painelli, A.; Katan, C.; Charlot, M.; Mireille, B. D. *J. Am. Chem. Soc.* **2006**, *128*, 15742−15755.
(33) (a) Shao, J. J.; Guan, Z. P.; Yan, Y. L.; Jiao, C. J.; Xu, Q. H.; Chi, C. Y. *J. Org. Chem.* **2011**, *76*, 780−790 and references therein. (b) Xu, C.; Webb, W. W. *J. Opt. Soc. Am. B* **1996**, *13*, 481−491. (c) Huang, Z. L.; Wang, H. Z. *Chem. Commun.* **2002**, 2400−2401. (d) Tian, N.; Xu, Q. H. *Adv. Mater.* **2007**, *19*, 1988−1991.
(34) (a) Li, L.; Tian, Y. P.; Yang, J. X.; Sun, P. P.; Wu, J. Y.; Wang, C. K.; Tao, X. T.; Jiang, M. H. *Chem.—Asian J.* **2009**, *4*, 668−680. (b) Wang, X. H.; Nguyen, D. M.; Yanez, C. O.; Rodriguez, L.; Ahn, H. Y.; Bondar, M. V.; Belfield, K. D. *J. Am. Chem. Soc.* **2010**, *132*, 12237−12239.
(35) Hrobarikova, V.; Hrobarik, P.; Gajdos, P. *J. Org. Chem.* **2011**, *76*, 3053−3068.
(36) Xu, C.; Zipfel, W.; Shear, J. B.; Williams, R. M.; Webb, W. W. *Proc. Natl. Acad. Sci. U.S.A.* **1996**, *93*, 10763−10768.
(37) Picot, A.; Malvolti, F.; Le Guennic, B.; Baldeck, P. L.; Williams, J. A. G.; Andraud, C.; Maury, O. *Inorg. Chem.* **2007**, *46*, 2659−2665.
(38) Picot, A.; D'Aléo, A.; Baldeck, P. L.; Grichine, A.; Duperray, A.; Andraud, C.; Maury, O. *J. Am. Chem. Soc.* **2008**, *130*, 1532−1533.
(39) Hai, Y.; Chen, J. J.; Zhao, P.; Lv, H. B.; Yu, Y.; Xu, P. Y.; Zhang, J. L. *Chem. Commun.* **2011**, *47*, 2435−2437.
(40) Dong, X. D.; Wang, X. Y.; Lin, M. X.; Sun, H.; Yang, X. L; Guo, Z. J. *Inorg. Chem.* **2010**, *49*, 2541−2549.
(41) Leydet, Y.; Bassani, D. M.; Jonusauskas, G.; McClenaghan, N. D. *J. Am. Chem. Soc.* **2007**, *129*, 8688−8689.
(42) Sheldrick, G. M. *SHELXL-97*, Program for Crystal Structures Refinement; University of Göttingen: Göttingen, Germany, 1997.
(43) Yang, L.; Feng, J. K.; Ren, A. M. *J. Org. Chem.* **2005**, *70*, 5987−5996.
(44) Wang, X. C.; Tian, Y. P.; Kan, Y. H.; Zuo, C. Y.; Wu, J. Y.; Jin, B. K.; Zhou, H. P.; Yang, J. X.; Zhang, S. Y.; Tao, X. T. *Dalton Trans.* **2009**, 4096−4103.
(45) Woo, H. Y.; Liu, B.; Kohler, B.; Korystov, D.; Mikhailovsky, A.; Bazan, G. C. *J. Am. Chem. Soc.* **2005**, *127*, 14721−14729.
(46) Cronstrand, P.; Luo, Y.; Ågren, H. *J. Chem. Phys.* **2002**, *117*, 11102−11106.
(47) Liu, Z. Q.; Fang, Q.; Wang, D.; Cao, D. X.; Xue, G.; Yu, W. T.; Lei, H. *Chem.—Eur. J.* **2003**, *9*, 5074−5084.
(48) Wenseleers, W.; Stellacci, F.; Meyer-Friedrichsen, T.; Mangel, T.; Marder, S. R.; Perry, J. W. *J. Chem. Phys. B* **2002**, *106*, 6853−6863.